JOURNAL OF ENVIRONMENTAL SCIENCES 93 (2020) 57–65

Available online at www.sciencedirect.com

ScienceDirect

www.elsevier.com/locate/jes

JES JOURNAL OF ENVIRONMENTAL SCIENCES

www.jesc.ac.cn

Enantioselective effects of imazethapyr residues on *Arabidopsis thaliana* metabolic profile and phyllosphere microbial communities

Qianqiu Zhao[1,3], *Wanyue Liu*[1,3], *Yan Li*[2], *Mingjing Ke*[2], *Qian Qu*[2], *Wenting Yuan*[2], *Xiangliang Pan*[1,2], *Haifeng Qian*[1,2,*]

[1] *Xinjiang Institute of Ecology and Geography, Chinese Academy of Sciences, Urumqi 830011, China*
[2] *College of Environment, Zhejiang University of Technology, Hangzhou 310032, China*
[3] *University of Chinese Academy of Sciences, Beijing 100049, China*

ARTICLE INFO

Article history:
Received 17 January 2020
Revised 4 March 2020
Accepted 4 March 2020
Available online 9 April 2020

Keywords:
Arabidopsis thaliana
Enantioselectivity
Chiral herbicides
Leaf metabolism
Phyllosphere microorganism

ABSTRACT

Imazethapyr (IM) is a widely used acetolactate synthase-inhibiting chiral herbicide. It has long-term residuals that may be absorbed by the human body through the edible parts of plants, such as vegetable leaves or fruits. Here, we selected a model plant, *Arabidopsis thaliana*, to determine the effects of R-IM and S-IM on its leaf structure, photosynthetic efficiency, and metabolites, as well as the structures of microorganisms in the phyllosphere, after 7 days of exposure. Our results indicated enantiomeric differences in plant growth between R-IM and S-IM; 133 μg/kg R-IM showed heavier inhibition of photosynthetic efficiency and greater changes to subcellular structure than S-IM. R-IM and S-IM also had different effects on metabolism and leaf microorganisms. S-IM mainly increased lipid compounds and decreased amino acids, while R-IM increased sugar accumulation. The relative abundance of *Moraxellaceae* human pathogenic bacteria was increased by R-IM treatment, indicating that R-IM treatment may increase leaf surface pathogenic bacteria. Our research provides a new perspective for evaluating the harmfulness of pesticide residues in soil, phyllosphere microbiome changes via the regulation of plant metabolism, and induced pathogenic bacterial accumulation risks.

Introduction

Pesticides increase the yield of agricultural products by killing insects, rodents, fungi, or unwanted plants (weeds) (Klier et al., 2019). In recent years, pesticide usage has increased dramatically, from 2011 to 2012, the annual use of pesticides worldwide was close to 6 billion pounds in weight (Atwood and Paisley-Jones, 2017). Of approximately 1590 globally used pesticides, 30% are chiral (Basheer, 2018), and chiral pesticides comprise nearly 40% of pesticide products in China (Asad et al., 2017). In agriculture, the pesticides inevitably enter the soil. However, the effects of pesticide residues in soil on plant foliar microbial communities remain unclear. Some reports have shown that crops can absorb pesticides through the roots or leaves and then transfer them to edible parts (Ghisi et al., 2019; Ke et al., 2020). In addition, the microorganisms in plant leaves form a complex microbial network that has beneficial or harmful effects on the host plant (Lu et al., 2018a,b), depending on the composition and function of leaf microorganisms. Microbe colonies on leaves can include bacteria that are pathogenic to plants and even humans, such colonies negatively effect on the host plants (Dees et al., 2015). In modern society, raw vegetables are becoming more

* Corresponding author:
E-mail: hfqian@zjut.edu.cn (H. Qian).

https://doi.org/10.1016/j.jes.2020.03.009
1001-0742/

prevalent in the human diet; dietary intake is one pathway for pathogens to enter animals or humans (Akoto et al., 2013).

The colonization of microorganisms in the phyllosphere is affected not only by environmental factors, such as radiation and pollution, but also by plant metabolites. Although few nutrients are present on the leaf surface, carbon sources found on the leaf surface, including carbohydrates, amino acids, organic acids, and sugar alcohols, affect the structures of microbial communities (Vorholt Julia, 2012). Plants produce primary and secondary metabolites through their own complex metabolic pathways when under stress. In the rhizosphere, root exudates shape soil microbial communities, which feedback-regulate plant growth (Pham et al., 2017; Michalet et al., 2013; Thijs et al., 2016; Lu et al., 2018a, 2018b).

It is well known that enantiomers of chiral pesticides have the same physical and chemical properties, but their bioavailability is different. Specifically, one enantiomer may have significant biological activity while others may have low or no biological activity (Qian et al., 2009). Imazethapyr (IM) is an imidazolinone herbicide with broad herbicidal activity that inhibits the growth of both monocotyledonous and dicotyledonous plants by blocking acetolactate synthase (ALS), thus affecting the synthesis of the branched-chain amino acids valine, leucine, and isoleucine, after its absorption by roots and leaves (Qian et al., 2015a; Bundt et al., 2015).

Previous research has confirmed the enantiomeric selectivity of IM. *R*-IM is more toxic to the growth of rice and *Arabidopsis thaliana* seedlings than S-IM (Qian et al., 2009, 2011a, 2013) and also affects plant flowering time and flowering organ development (Qian et al., 2014a, 2015a). IM has a long residual time in soil and its long-term use can cause residual accumulation that damages non-target plants and crops (Bundt et al., 2015). Li et al. (2015) showed that IM residue exerted stress on the succeeding rapeseed. In addition, IM induces the accumulation of reactive oxygen species (ROS) in rice and *A. thaliana*, which seriously hinders the normal operation of glucose metabolism (Qian et al., 2011b). In our latest studies, the application of IM by spraying was shown to destroy the leaf structure, reduce photosynthetic efficiency, inhibit antioxidant enzyme activity, and change the microbial compositions and structures on the leaf surface. IM could increase the number of pathogenic bacteria on the leaves by spraying (Liu et al., 2019).

Root exudates can respond to biotic and abiotic stresses in the rhizosphere, and regulate rhizosphere microorganisms to respond stress via chemical communication (Liu et al., 2020). We hypothesized that when the pollutants at the soil interface were absorbed by root, it also changes the compounds and microorganism in the phyllosphere. We used *A. thaliana* to study plant leaf physiological changes in when IM was absorbed by the plant roots and uncovered the relationship between phyllosphere microbial communities and leaf metabolism. Our research provides a new perspective for evaluating the harmfulness of pesticide residues in soil, phyllosphere microbiome changes via the regulation of plant metabolism, and induced pathogenic bacterial accumulation risks.

1. Materials and methods

1.1. Plant material and growth conditions

Colombia *A. thaliana* (Col-0) was selected as the experimental organism. The seeds were sterilized with 75% ethanol for 1 min, washed with sterile water six or seven times, sterilized with 2.5% (*V*/*V*) sodium hypochlorite for 15 min, and washed again with sterile water six or seven times to remove sodium hypochlorite. After sterilization, the seeds were allowed to absorb moisture and were stored at 4 °C for two days to germinate. The seeds were then sown on a Murashige and Skoog (MS) medium, with the addition of 0.8% (*W*/*V*) agarose and 3% (*W*/*V*) sucrose to the MS medium (Qian et al., 2013). Fourteen days after sowing, the seedlings were transferred into a culture box filled with 30 g natural soil collected on the campus of the Zhejiang University of Technology, China (30 17′ 45.11″ N, 120 09′ 50.07″ E). The culture box measured approximately 12 cm × 12 cm, and nine culture points were evenly distributed in each box. Holes at the bottom of the culture points allowed the permeation of MS nutrient solution (initial pH 5.6 ± 0.05, composition as described in Zhu et al. (2013)) from bottom to top. The culture boxes were held at room temperature (25 ± 0.5 °C) with cyclic exposure to 12 h light (300 mmol/m^2 s)/12 h darkness for two weeks, allowing microorganisms to colonize the leaves. One pair of enantiomers (*R*- and *S*-IM) were separated from the racemic IM mixture (CAS number: 1344-28-1, China) by Shanghai Chiralway Biotech Co., Ltd. The *R*- and *S*-IM powders were dissolved in acetone, and the concentration was determined using high-performance liquid chromatography (HPLC). According to our previous report on the adsorption and degradation of IM in soil (Qian et al., 2015b), 300 mL of MS nutrient solution with 40 μg/L of the *R*- or *S*-IM were added into 90 g of potting soil respectively. The final concentration of IM enantiomers was 133 μg/kg dry soil, which is known to significantly inhibit *A. thaliana* growth (Qian et al., 2015b; Liu et al., 2019). Leaf samples were collected immediately after 7 days treatment for microorganism16S rRNA gene analysis and metabolomics analysis. Four repetitions were prepared for each treatment condition, and every replicate consisted of nine plantlets.

1.2. Water content and chlorophyll fluorescence in plant tissue measurement

Some leaf samples were used to measure the water content. Whole fresh plants were dried at 65 °C for 48 h (*WC*, %):

$$WC = [(X_0 - X_n)/X_0] \times 100\%$$

In the above formula, X_0 (g) represents the fresh weight, and X_n (g) represents the dry weight.

Other *A. thaliana* plants growing in the culture box were placed in a dark environment for more than 30 min and then tested for their chlorophyll fluorescence indices, either in the dark or under very low light intensity. A dual PAM-100 chlorophyll fluorometer (Heinz Walz, Effeltrich, Germany) was used to measure the minimum fluorescence F_0. The instrument was given a saturation pulse (10,000 μmol photons/m^2 s) to determine the chlorophyll fluorescence of the leaves. The effective photochemical quantum yield of PSII is represented by Y(II), Y(NO) and Y(NPQ) represent the quantum yields of non-photo-induced and non-photochemical fluorescence quenching, ETR represents the relative electron transfer rate (Qian et al., 2014b; Sun et al., 2016).

1.3. Scanning electron microscopy (SEM) and transmission electron microscopy (TEM) analyses

After 7 days of exposure, *A. thaliana* leaf samples were collected and cut along the veins. The samples were first fixed with glutaraldehyde (2.5%) in a phosphate buffer (0.1 mol/L, pH = 7.0) for 4 h, washed three to four times in the phosphate buffer for 15 min at each step. Then, post-fixed with OsO_4 (1%) in phosphate buffer for 2 h, and rinsed three times for 15 min again. The samples were dehydrated by a graded series of ethanol solutions (30%, 50%, 70%, 80%, 90% and 95%)

for about 15 min at each step. After dehydration, the samples were observed by scanning electron microscopy (SEM; Hitachi Model SU-8010, Japan) after coating with gold–palladium.

Other samples were selected and immersed in a mixture of absolute acetone and Spurr resin in different proportions (1:1 for 1 h; 1:3 for 3 h). The samples were held overnight at room temperature. The leaf samples were then placed in Spurr resin, heated to 70 °C for 9 h, and then observed using a Hitachi Model H-7650 transmission electron microscope (TEM) after sectioning and staining.

1.4. *DNA extraction and 16S rRNA gene amplicon sequencing*

Total genomic DNA was extracted from 0.25 g of sample using the MO BIO PowerSoil DNA Isolation Kit (BIOMIGA, USA) according to the manufacturer's protocols. According to the concentration, the acquired DNA samples were diluted to 1 ng/μL using sterile water. 16S rRNA genes of distinct regions were amplified using the specific primers 314F (5′-CCTACGGGNGGCWGCAG-3′) and 805R (5′-GACTACHV GGGTATCTAATCC-3′). All polymerase chain reaction (PCR) processes were performed with the KAPA HiFi^{TM} HotStart ReadyMix (2X). The PCR product was confirmed by using 1% agarose gel electrophoresis. The amplified products were purified with Beckman DNA Clean Beads and quantified by a Qubit 2.0 fluorometer (Invitrogen, Carlsbad, CA, USA). The enriched library was loaded in an Ion 530^{TM} Chip and sequenced on an Ion S5TM platform (Thermo Fisher Scientific, Waltham, MA; Zhejiang TianKe Hitech Development Co., Ltd., Hangzhou, China), generating 400 bp/600 base pair (bp) single-end reads. Single-end reads were assigned to samples based on their unique barcodes and truncated by cutting off the barcodes and primer sequences for data splitting. The raw reads were filtered, according to Cutadapt, in order to acquire high-quality reads (Martin, 2011). Sequences with ≥ 97% similarity were assigned to the same operational taxonomic units (OTUs). Alpha diversity was applied in analyzing the complexity of species diversity for a sample through six indices, including Observed-species, Chao1, Shannon, Simpson, ACE, and Good-coverage. All these indices in our samples were calculated with QIIME (Version 1.9.1) and displayed with R software (Version 3.2.2). Principle coordinate analysis (PCoA) was displayed by the vegan package, stat packages, and ggplot2 package in R software (Version 3.3.0).

1.5. *Gas chromatography and mass spectrometry analyses of* A. thaliana *leaf metabolites*

For preparation, 10 mg of the sample was added to 5 μL of 3 mg/mL of myristic acid-d27 solution, and then to 1000 μL of extractant (acetonitrile/isopropanol/water, 3/3/2, V/V). This mixture was vortexed for 1 min. The samples were then centrifuged at 13,000 r/min for 5 min at 4 °C. About 800 μL of the supernatant was dried using nitrogen and lyophilized for 30 min in a lyophilizer. In a two-step derivatization, 20 μL of 40 mg/mL methoxamine hydrochloride/pyridine was added and derivatized at 30 °C for 90 min, and then 90 μL of N-methyl-N(trimethylsilyl) trifluoroacetamide (MSTFA) containing 1% trimethylchlorosilane (TMCS) was added and derivatized for 30 min. The samples were then centrifuged again at 13,000 r/min for 5 min at 4 °C and 60 μL of the supernatant was collected for testing. A quality control (QC) sample was also prepared as follows: the same volume from the prepared sample was collected and mixed into a large sample, then divided into six QC samples to monitor instabilities of instrument precision. Three QC samples collected before sampling were used to monitor the precision of the instrument, and one QC sample was tested every six samples to monitor the stability of the instrument.

The derivatized samples were analyzed by using an Agilent 7890A gas chromatography (GC) system coupled to an Agilent 5975C mass-selective detector (MSD) with a DB-5MS fused-silica capillary column (30 m × 250 μm internal diameter with 0.25-μm film). The injection volume was 1 μL with the injector temperature of 250 °C and the MSD interface temperature of 230 °C in split mode; the split ratio was 10:1. The initial oven temperature was 60 °C, ramped to 300 °C at a rate of 10 °C/min, and held at 300 °C for 10 min. The selected temperatures of the MS quadrupole and ion source (electron impact) were 150 and 250 °C, respectively. Mass data were acquired in a full-scan mode (*m/z* 50–500). GC MS raw data files were converted into NetCDF format by Agilent Chrom Station software (Agilent Technologies, USA) and then preprocessed by the *erah* package in R. Each metabolite in the samples was identified simultaneously by combining the retention time (RT) and *m/z* data. The online GMD database was used to annotate the metabolites by matching the *m/z* data of samples with those from database. Metabolites with ≥ 80 similarity were retained. The intensity of peak data was further processed by "erah" R package, and then used to compare the differences between metabolites of the treatment group and the control group.

The table of metabolite results was imported into SIMCA-P+14.0 (U Metrics, UME, Sweden) and the experimental groups were named. The orthogonal partial least-squares discrimination analysis (OPLS-DA) model was used to analyze the differences between the groups. The variables important in projection (VIP) >1 were considered variance variables in the OPLS-DA analysis. The *p*-value was calculated according to the T-test to evaluate the statistical significance of the different variables and then adjusted using the methods described by Benjamini and Hochberg (1995) (Appendix A, *Table S1*); variables with *p* values of less than 0.05 were considered to show significant differences. Metabolic pathway analysis was performed by MetaboAnalyst 4.0.

2. Results and discussion

2.1. *Effects of IM enantiomers on plant water content and photosynthetic efficiency*

We measured the plant water content after 7 days of exposure to the IM enantiomers. Compared to the control group, the plant water content showed no significant change with *S*-IM treatment, while it was decreased by 1.3% after *R*-IM treatment (Fig. 1a), Even though this amount of reduction is small, it is still significant after *R*-IM treatment, indicating that *R*-IM treatment has a negative impact on plant water content. This is consistent with previous results from the direct spraying of IM on foliage (Liu et al., 2019).

We used five chlorophyll fluorescence parameters to evaluate the enantioselectivity of IM on photosynthesis, including Y(II), Y(NPQ), Y(NO), Fv/Fm, and ETR. Our data demonstrated that *R*-IM and *S*-IM showed different enantioselective effects on plant photosynthesis (Fig. 1b). This phenomenon is displayed by the following results: (1) the Y(II) value in the *R*-IM treatment was down-regulated by 53.16% compared to that of the control group, while that in the *S*-IM group was decreased by only 6%; (2) the Y(NO) values of the *R*-IM and *S*-IM treatment groups were increased by 81.93% and 49.77% relative to that of the control group, respectively and (3) Y(NPQ) in the *R*-IM treatment group was increased by 10.46%, but decreased by 6.43% in the *S*-IM treatment group. The proportional relationships of the three parameters Y(II), Y (NPQ), and Y(NO) reflect the ability of the plant to utilize energy (Klug Hammer

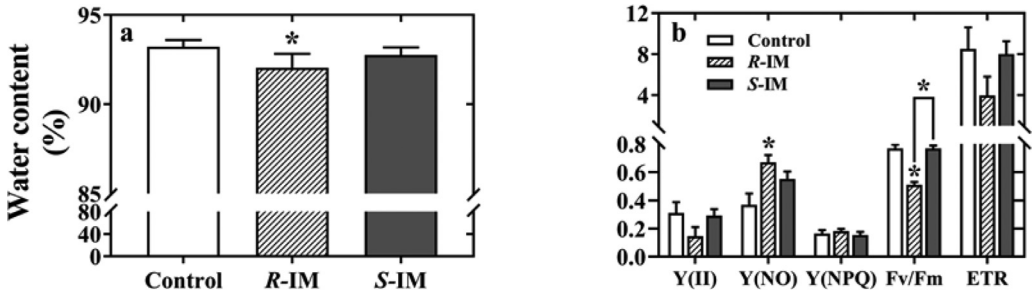

Fig. 1 – Effects of IM enantiomers on (a) water content and (b) chlorophyll fluorescence in plant tissue measurement after 7 days of control and IM treatment (*R*-IM, *S*-IM). * Represents that compared with the control group, the treatment group are significant ($p < 0.05$).

and Schreiber, 2008; Liu et al., 2015). The value of Y(II) decreased significantly, which reflected the inhibition by *R*-IM of PSII photochemical energy utilization and electron transfer chains in thylakoids. The high Y(NO) value indicated that ΔpH thylakoids were not completely established, possibly corresponding to the accumulation of excess electrons and the production of ROS (Sun et al., 2016; Liu et al., 2019). This indicates that PSII's ability to process energy is disturbed and that the enantioselectivity causes irreversible damage (Chen et al., 2016). The Fv/Fm value in the *R*-IM treatment group was down-regulated by 66.36% compared to that in the control group, while no significant difference appeared between those of the *S*-IM treatment and control groups this also supports enantioselectivity. Finally, compared with the control group, the ETR value of the *R*-IM treatment group was decreased by 53.33% and that of the *S*-IM group was decreased by only 5.88%. However, there was no significant difference between the treatment group and the control group. *R*-IM damaged the photosynthetic apparatus and electron transfer process more seriously than *S*-IM, resulting in the decrease of light energy conversion efficiency (Xia et al., 2014). The differences of these results indicate that *R*-IM heavily affects the photosynthetic rate of plants.

2.2. *Observations of the leaf cell subcellular structure with TEM and SEM*

Based on SEM observations, mesophyll cells were affected to different degrees after 7 days of *S*-IM and *R*-IM treatment (Fig. 2). Compared to that in the control group, the arrangement of epidermal cells in the IM treatment groups is tighter and the stomatal closure rate is higher. The changes of mesophyll cell deformation and stomatal closure rate after *R*-IM treatment are the most obvious among the three groups. The effects observed in the *S*-IM treatment group are between those in the control group and *R*-IM group (Fig. 2a). The difference in effect between the enantiomers is similar to that achieve in spraying racemic IM directly on the leaf surface relative to the control (Liu et al, 2019).

After 7 days of IM treatment, the number of starch granules in the chloroplasts was increased by about 45%, especially after *R*-IM treatment (Fig. 2b). A significant increase in the number of starch particles in chloroplasts causes the thinning of thylakoid particles, which play an important role in light absorption and electron transfer (Tan et al., 2014). The results showed that IM treatment increased the number and size of starch particles and affected the structure of the thylakoid layer in the chloroplasts. This may affect the photosynthesis of the leaves, which is consistent with previous studies (Qian et al., 2011b; Qu et al., 2019). However, this is the first time that IM has been found to affect leaf structure when absorbed through the roots of plants.

2.3. *Metabolic response of* A. thaliana *leaves to* S*-IM and* R*-IM*

A total of 77 metabolites were ultimately identified from the extracts of *A. thaliana* leaves after *S*-IM or *R*-IM treatment compared with the control groups, including 24 sugars, 18 organic acids, nine amino acids, 12 alcohols, five hydrocarbons, three esters, and six other compounds. In order to maximize the separation between groups, we performed the orthogonal partial least squares (OPLS) analysis based on differential metabolites (Fig. 3a). The results showed that both the *R*-IM group and *S*-IM group showed different metabolic profiles relative to the control group of *A. thaliana* leaves. In order to further analyze the effects of *R*-IM and *S*-IM treatment on the metabolites, we selected 17 different metabolites with VIP > 1 and $p < 0.05$ for visual display. IM treatment significantly changed these metabolites, which included three sugars, four amino acids, two alcohols, two lipids, two sugar acids, and four other substances (organic acids, inorganic acids, alkaloids, amides.) (Fig. 3b). From the results, IM treatment caused the accumulation of carbohydrates in the leaves. Most sugars, such as galactose and fructose, accumulated in *R*-IM treatment were higher in concentration than they were in the *S*-IM group. Sugar usually accumulates in plants under stress (Shi et al., 2018; Ke et al., 2018). The accumulation of carbohydrates may indicate that plants consume carbohydrates to produce energy for the synthesis of defense substances such as phenols after stress (Mikulic-Petkovsek et al., 2013; Bowne et al., 2012). Surprisingly, compared to the control group, the amino acid contents of the treatment groups in the selected significantly different metabolites were reduced, especially with *S*-IM treatment. Chen et al. (2017) obtained similar results in the study of *A. thaliana* exposed to *S*-dichlorprop, which significantly reduced the concentration of several amino acids. In addition, amines were up-regulated in the *R*-IM treatment group. Lipid substances such as heptanoic acid and butyric acid were accumulated in the treatment groups; *S*-IM caused greater lipid accumulation than *R*-IM. Lipids are important substances for energy storage and signal transmission in organisms. When plants are stressed, lipid accumulation can assist in cell membrane reconstruction to address plant cell damage (Parviz Moradi et al., 2017) or algal cells (Zhang et al., 2019), which could be one mechanism by which *S*-IM toxicity to plant cells is alleviated.

2.4. *Changes of microbial communities on leaf surface*

In order to analyze the compositions and changes in bacterial communities on the surfaces of *A. thaliana* leaves, we sequenced the genomes of each leaf. We obtained a total of 50,557–54,588 raw reads from the leaf samples of the control and two treatment groups and clustered the sequences into

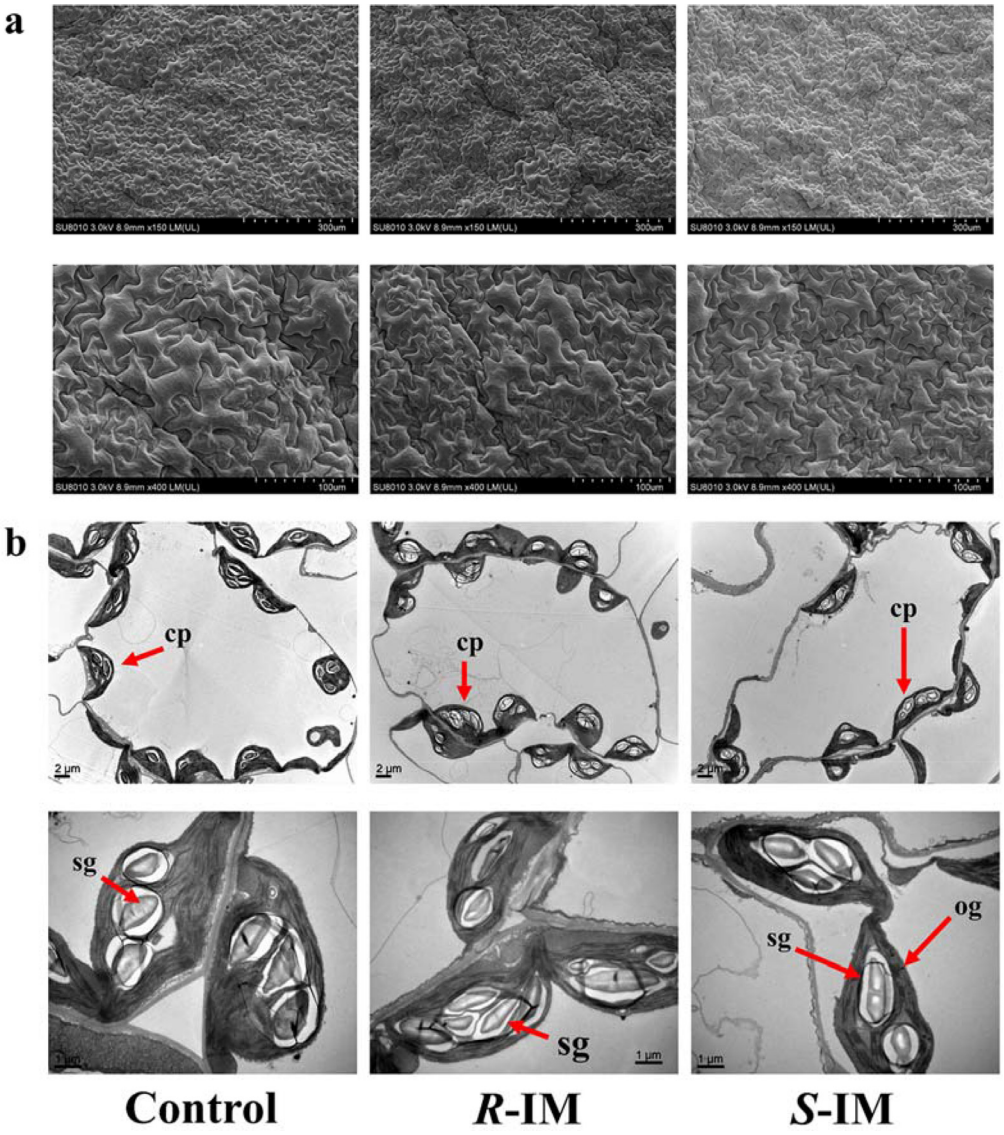

Fig. 2 – Changes of leaves morphology and subcellular structure in *A. thaliana* after 7 days of IM treatment. (a) Leaf surface morphologies; (b) Mesophyll cell structure. sg: starch granule; og: osmiophilic granule.

OTUs with 97% identity, and then annotated the representative sequences of OTUs. The good-coverage index of the collected samples was greater than 99.8%, proving that the sequencing depth was sufficient to cover most OTUs in all samples. Compared to the indices in the control group, the Simpson, Shannon, and Chao1 evenness indices in the treatment groups were higher. The Simpson and Shannon indices were additionally higher in the *S*-IM treatment group than in the *R*-IM treatment group (Fig. 4). Briefly, compared with the control group, α diversity indices based on the OTUs in the treatment group were increased, indicating that the bacterial community structure was affected by the IM enantiomer, and that *R*-IM and *S*-IM showed different effects. These results clearly demonstrate that IM enantiomers affect the diversity of bacterial communities to different extents.

Based on the changes in bacterial abundance detected by OTU, we further concentrated on variations at specific taxonomic levels. First, after 7 days of IM treatment, the bacterial taxa in the treatment and the control group remained relatively stable at the phylum level. Amongst the three groups, *Proteobacteria* accounts for 63.5%–72.9%, which is the most abundant phylum. In the treatment group, *Actinobacteria* (1.7%–2.0%) replaced *Bacteroidetes* (1.1%–1.2%) in the control group to become the second-most abundant phylum (Fig. 5a). At the family level, the effects of *R*-IM and *S*-IM treatments on bacterial abundance showed differences. The abundance of the dominant *Pseudomonadaceae* was decreased by 21.7% and 41% relative to the control after *R*-IM and *S*-IM treatment, respectively (Fig. 5b).

In the family of *Pseudomonaceae*, some species in the genus showed protective effects on stimulating plant growth, resisting pests, and bioremediation (Munir et al., 2019; Aydogan et al., 2018). For example, Chu et al. (2019) reported that *Pseudomonas PS01* can help *A. thaliana* to develop salt tolerance. The decrease of *Pseudomonas* may indicate that IM adversely affects the stress resistance of leaves. However, the *R*-IM treatment increased the abundance of *Moraxellaceae* by 56%, while the *S*-IM treatment decreased the abundance of *Moraxellaceae* by44% (Fig. 6c). In the family of *Moraxellaceae, Acinetobacter* is an opportunistic pathogen that can infect people with low immune function and is a serious threat to human health (Howard et al., 2012; Hassan et al., 2017). Therefore, edible

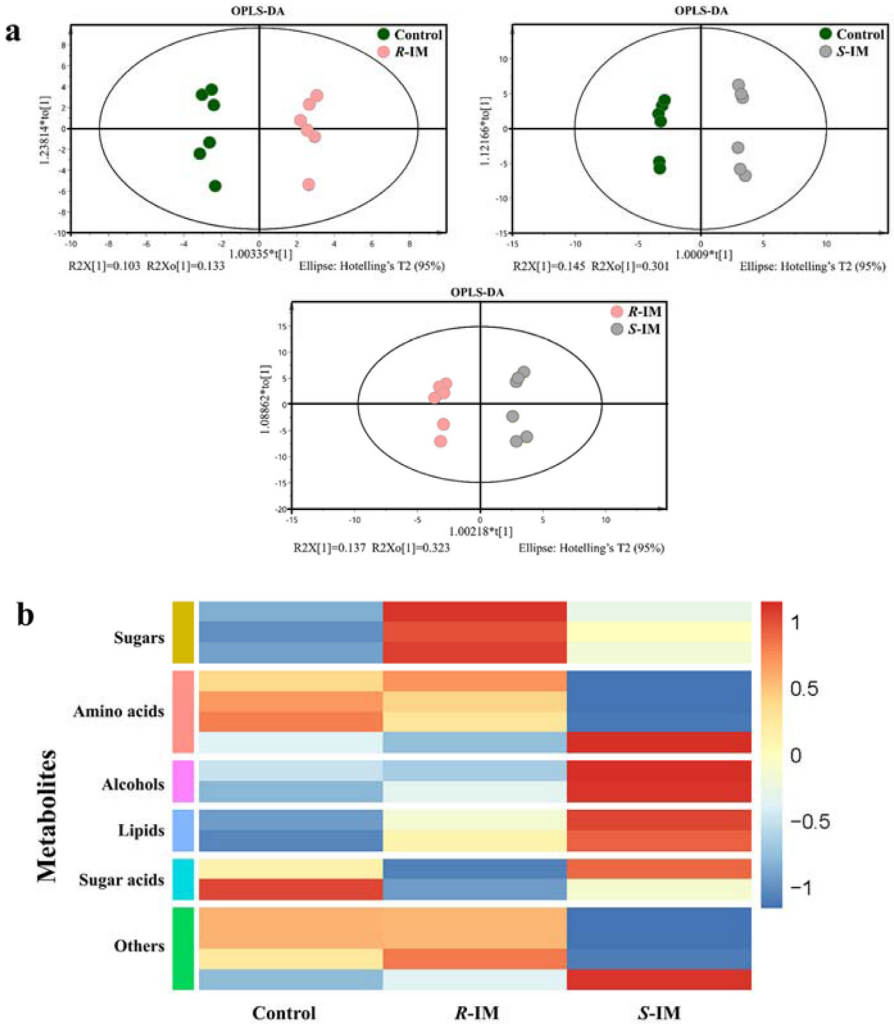

Fig. 3 – (a) Orthogonal partial least squares (OPLS) analysis of leaf metabolites of control and IM-treated groups. Points with different colors represent samples from the different groups collected after 7 days. (b) Heatmap analysis of changes in leaf metabolites of control and IM-treated (R-IM, S-IM) groups.

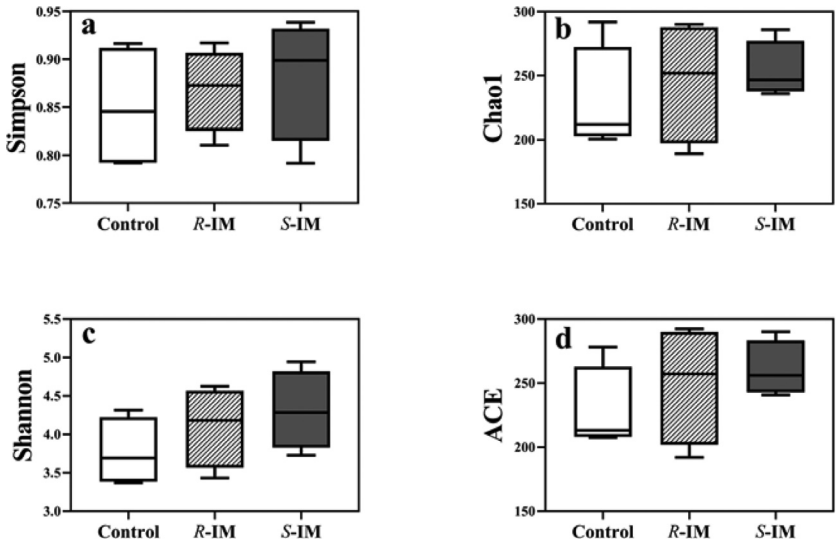

Fig. 4 – Alpha indices including (a) Simpson, (b) Chao1, (c) Shannon, and (d) ACE after 7 days of control and IM treatment (R-IM, S-IM).

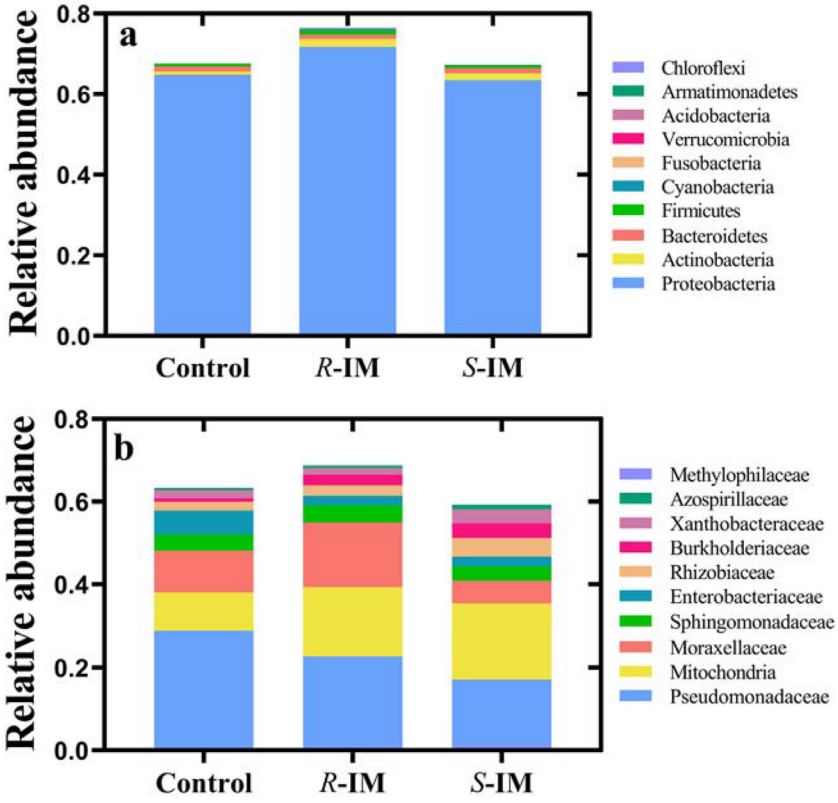

Fig. 5 – Relative abundance of 16S rRNA gene of (a) main phyla and (b) families present in the bacterial communities after 7 days of control and IM treatment (R-IM, S-IM).

leaves with increased pathogen abundance could threaten human health.

2.5. *Correlation analysis of metabolites and phyllosphere microorganism*

The foliar environment is highly variable and considered a relatively harsh habitat. In addition, the foliar environment can provide fewer nutrients, nutrient availability is an important factor in limiting the proliferation of microorganisms (Souza et al., 2015). Leaf colonists must endure such stresses.

In this study, we analyzed the correlations between differential metabolites and microbial abundance. Based on the correlation heat map between microorganism family level TOP10 and differential metabolites (Fig. 6), sugar had a positive correlation with most bacteria but a negative correlation with *Enterobacteriaceae*. Except for sarcosine, amino acid metabolites and *Moraxellaceae, Sphingomonadaceae, Pseudomonadaceae,* and *Enterobacteriaceae* were positively correlated. The two lipid substances (heptanoic acid, butanoic acid) were negatively correlated with *Pseudomonadaceae* and *Enterobacteriaceae*. IM treatment, especially S-IM treatment, down-regulated several amino acid metabolites, thus causing a decrease in nitrogen sources available to microorganisms. Vorholt (2012) reported that in fertile plants, the availability of nitrogen is the second limiting factor for microbial communities besides carbon. In our research, microorganisms with nitrogen fixation ability (Fig. 6b), including *Xanthobacteraceae, Rhizobiaceae, Azospirillaceae*, and *Burkholderiaceae*, formed colonies and became dominant strains (Aanderud et al., 2018; Souza et al., 2015; Ju et al., 2019; He et al., 2018; Fei et al., 2020; Fürnkranz et al., 2008). On the other hand, past studies showed that many bacteria related to non-leguminous plants, including *Azospirillaceae* and *Burkholderiaceae*, promoted plant growth (Souza et al., 2015; Govindarajan et al., 2008). However, the interactions between microorganisms and leaf metabolites are more complex, and the specific mechanisms of influence require further exploration.

3. Conclusion

In agriculture, applied pesticides accumulate and remain in the soil. We speculated that even if pesticides were to cause only minor damage to plant growth, for example, by affecting the water content, leaf subcellular structure, and photosynthetic level, they would still affect the phyllosphere microbial communities and leaf metabolites, which are often overlooked. In this study, we researched the effects of IM soil application on the physiological activities of *A. thaliana* leaves, microorganism communities, and metabolites in the phyllosphere, and the correlation between metabolites and microorganisms in the phyllosphere. Our results showed that the soil application of IM, especially the R-IM enantiomer, inhibited leaf water content, affected leaf cell structure, and reduced plant photosynthetic efficiency. It also affected the metabolites and microbial communities formed on the leaf surfaces. This study thus improves the current understanding of the differences in the effects of enantiomeric IM residues on the physiological activities and microorganisms of plant leaves.

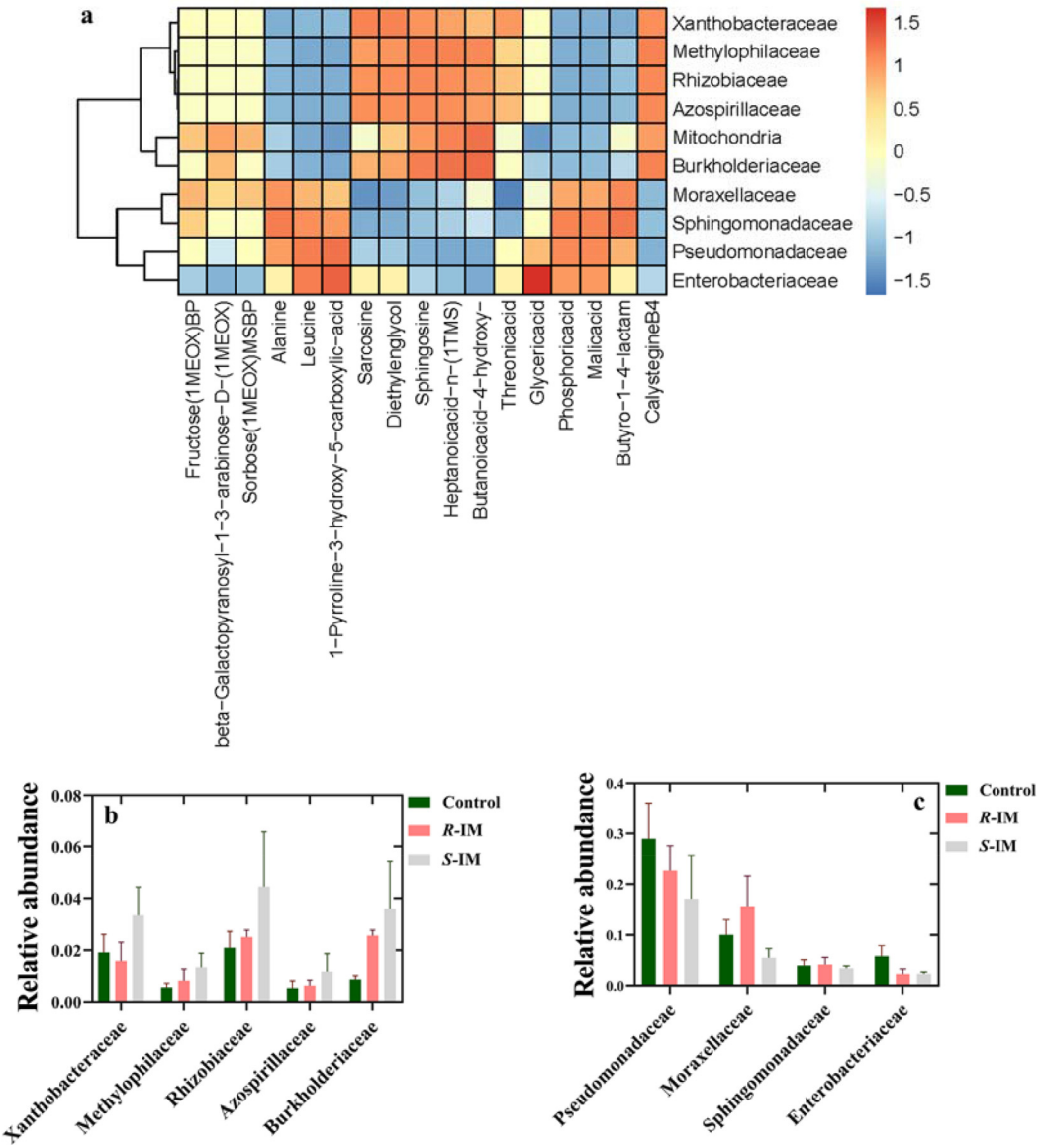

Fig. 6 – The correction analysis between the TOP10 of OTUs (at family level) and leaf metabolites. Only corrections ≥0.5 are presented (positive correlation: red; negative correlation: blue). (a) OTUs and metabolites are notably changed in the control group and IM treatment groups. (b) The relative abundance (family level) of microorganisms is negatively correlated to most amino acids and alcohols. (c) The relative abundance (family level) of microorganisms is positively correlated to most amino acids and alcohols. (For interpretation of the references to color in this figure legend, the reader is referred to the web version of this article.)

Acknowledgments

This work was supported by the National Natural Science Foundation of China (Nos. 21777144, 21976161), the CAS Pioneer Hundred Talents Program (H.F. Qian), and the Xinjiang Uighur Autonomous Region Talent Project (H.F. Qian).

Appendix A. Supplementary data

Supplementary material associated with this article can be found, in the online version, at doi:10.1016/j.jes.2020.03.009.

REFERENCES

Aanderud, Z.T., Saurey, S., Ball, B.A., Wall, D.H., Barrett, J.E., Muscarella, M.E., et al., 2018. Stoichiometric shifts in soil C: N: P promote bacterial taxa dominance, maintain biodiversity, and deconstruct community assemblages. Front. Microbiol. 9, 1401.

Akoto, O., Andoh, H., Darko, G., Eshun, K., Osei-Fosu, P., 2013. Health risk assessment of pesticides residue in maize and cowpea from Ejura, Ghana. Chemosphere 92 (1), 67–73.

Asad, M.A.U., Lavoie, M., Song, H., Jin, Y., Fu, Z., Qian, H., 2017. Interaction of chiral herbicides with soil microorganisms, algae and vascular plants. Sci. Total Environ. 580, 1287–1299.

Atwood, D., Paisley-Jones, C., 2017. Pesticides Industry Sales and Usage: 2008–2012 Market Estimates. USEPA.

Aydogan, E.L., Moser, G., Müller, C., Kämpfer, P., Glaeser, S.P., 2018. Long-term warming shifts the composition of bacterial communities in the phyllosphere of *Galium album* in a permanent grassland field–experiment. Front. Microbiol. 9, 144.
Basheer, A.A., 2018. Chemical chiral pollution: impact on the society and science and need of the regulations in the 21st century. Chirality 30 (4), 402–406.
Benjamini, Y., Hochberg, Y., 1995. Controlling the false discovery rate: a practical and powerful approach to multiple testing. J. R. Stat. Soc. 57 (1), 289–300.
Bowne, J.B., Erwin, T.A., Juttner, J., Schnurbusch, T., Langridge, P., Bacic, A., et al., 2012. Drought responses of leaf tissues from wheat cultivars of differing drought tolerance at the metabolite level. Mol. Plant. 5 (2), 418–429.
Bundt, A.C., Avila, L.A., Pivetta, A., Agostinetto, D., Dick, D.P., Burauel, P., 2015. Imidazolinone degradation in soil in response to application history. Planta Daninha 33 (2), 341–349.
Chen, Z., Zou, Y., Wang, J., Li, M., Wen, Y., 2016. Phytotoxicity of chiral herbicide bromacil: enantioselectivity of photosynthesis in *Arabidopsis thaliana*. Sci. Total Environ. 548, 139–147.
Chen, Z., Wang, J., Chen, S., Wen, Y., 2017. Enantioselective disturbance of chiral herbicide dichlorprop to nitrogen metabolism of *Arabidopsis thaliana*: regular analysis and stable isotope attempt. Sci. Total Environ. 603, 533–540.
Chu, T.N., Tran, B.T.H., Bui, L.V., Hoang, M.T.T., 2019. Plant growth-promoting rhizobacterium *Pseudomonas* PS01 induces salt tolerance in *Arabidopsis thaliana*. BMC Res. Notes. 12 (1), 11.
Dees, M.W., Lysøe, E., Nordskog, B., Brurberg, M.B., 2015. Bacterial communities associated with surfaces of leafy greens: shift in composition and decrease in richness over time. Appl. Environ. Microbiol. 81 (4), 1530–1539.
Fei, Y., Huang, S., Zhang, H., Tong, Y., Wen, D., Xia, X., et al., 2020. Response of soil enzyme activities and bacterial communities to the accumulation of microplastics in an acid cropped soil. Sci. Total Environ. 707, 135634. doi:10.1016/j.scitotenv.2019.135634.
Fürnkranz, M., Wanek, W., Richter, A., Abell, G., Rasche, F., Sessitsch, A., 2008. Nitrogen fixation by phyllosphere bacteria associated with higher plants and their colonizing epiphytes of a tropical lowland rainforest of Costa Rica. ISME J. 2 (5), 561.
Ghisi, R., Vamerali, T., Manzetti, S., 2019. Accumulation of perfluorinated alkyl substances (PFAS) in agricultural plants: a review. Environ. Res. 169, 326–341.
Govindarajan, M., Balandreau, J., Kwon, S.W., Weon, H.Y., Lakshminarasimhan, C., 2008. Effects of the inoculation of *Burkholderia vietnamensis* and related endophytic diazotrophic bacteria on grain yield of rice. Microb. Ecol. 55 (1), 21–37.
Hassan, K.A., Pederick, V.G., Elbourne, L.D., Paulsen, I.T., Paton, J.C., McDevitt, C.A., et al., 2017. Zinc stress induces copper depletion in *Acinetobacter baumannii*. BMC Microbiol. 17 (1), 59.
He, T., Li, Z., Xie, D., Sun, Q., Xu, Y., Ye, Q., et al., 2018. Simultaneous nitrification and denitrification with different mixed nitrogen loads by a hypothermia aerobic bacterium. Biodegradation 29 (2), 159–170.
Howard, A., O'Donoghue, M., Feeney, A., Sleator, R.D., 2012. *Acinetobacter baumannii*: an emerging opportunistic pathogen. Virulence 3 (3), 243–250.
Ju, H., Zhu, D., Qiao, M., 2019. Effects of polyethylene microplastics on the gut microbial community, reproduction and avoidance behaviors of the soil springtail, *Folsomia candida*. Environ. Pollut. 247, 890–897.
Ke, M., Qu, Q., Peijnenburg, W.J.G.M., Li, X., Zhang, M., Zhang, Z., et al., 2018. Phytotoxic effects of silver nanoparticles and silver ions to *Arabidopsis thaliana* as revealed by analysis of molecular responses and of metabolic pathways. Sci. Total Environ. 644, 1070–1079.
Ke, M., Li, Y., Qu, Q., Ye, Y., Peijnenburg, W.J.G.M., Zhang, Z., et al., 2020. Offspring toxicity of silver nanoparticles to *Arabidopsis thaliana* flowering and floral development. J. Hazard. Mater. 386, 121975.
Klier, B., Häfner, E., Albert, H., Binder, G., Knödler, M., Kühn, M., et al., 2019. Pesticide residues in herbal drugs: evaluation of a database. J. Appl. Res. Med. Aromat. Plants 15, 100223.
Klughammer, C., Schreiber, U., 2008. Complementary PS II quantum yields calculated from simple fluorescence parameters measured by PAM fluorometry and the saturation pulse method. PAM Appl. Notes 1 (2), 201–247.
Li, X., Li, G., Xie, L., LI, Y., Chen, X., 2015. Effects of imazethapyr residue on physiological indices of succeeding crop of rapeseed. Agrochemicals 54 (9), 671–673.
Liu, H., Zhang, S., Zhang, X., Chen, C., 2015. Growth inhibition and effect on photosystem by three imidazolium chloride ionic liquids in rice seedlings. J. Hazard. Mater. 286, 440–448.
Liu, W., Ke, M., Zhang, Z., Lu, T., Zhu, Y., Li, Y., et al., 2019. Effects of imazethapyr spraying on plant growth and leaf surface microbial communities in *Arabidopsis thaliana*. J. Environ. Sci. 85, 35–45.
Liu, W., Zhao, Q., Zhang, Z., Li, Y., Xu, N., Qu, Q., et al., 2020. Enantioselective effects of imazethapyr on *Arabidopsis thaliana* root exudates and rhizosphere microbes. Sci. Total Environ. 716, 137121. doi:10.1016/j.scitotenv.2020.137121.
Lu, T., Ke, M., Peijnenburg, W.J.G.M., Zhu, Y., Zhang, M., Sun, L., et al., 2018a. Investigation of rhizospheric microbial communities in wheat, barley, and two rice varieties at the seedling stage. J. Agric. Food Chem. 66 (11), 2645–2653.
Lu, T., Ke, M., Lavoie, M., Jin, Y., Fan, X., Zhang, Z., et al., 2018b. Rhizosphere microorganisms can influence the timing of plant flowering. Microbiome 6 (1), 231.
Martin, M., 2011. Cutadapt removes adapter sequences from high–throughput sequencing reads. EMBnet J. 17 (1), 10–12.
Michalet, S., Rohr, J., Warshan, D., Bardon, C., Roggy, J.C., Domenach, A.M., et al., 2013. Phytochemical analysis of mature tree root exudates in situ and their role in shaping soil microbial communities in relation to tree N-acquisition strategy. Plant Physiol. Biochem. 72, 169–177.
Mikulic–Petkovsek, M., Schmitzer, V., Slatnar, A., Weber, N., Veberic, R., Stampar, F., et al., 2013. Alteration of the content of primary and secondary metabolites in strawberry fruit by *Colletotrichum nymphaeae* infection.. J. Agric. Food Chem. 61 (25), 5987–5995.
Moradi, P., Ford–Lloyd, B., Pritchard, J., 2017. Metabolomic approach reveals the biochemical mechanisms underlying drought stress tolerance in Thyme. Anal. Biochem. 527, 49–62.
Munir, I., Bano, A., Faisal, M., 2019. Impact of phosphate solubilizing bacteria on wheat (*Triticum aestivum*) in the presence of pesticides. Braz. J. Biol. 79 (1), 29–37.
Pham, H.N., Michalet, S., Bodillis, J., Nguyen, T.D., Nguyen, T.K.O., Le, T.P.Q., et al., 2017. Impact of metal stress on the production of secondary metabolites in *Pteris vittata* L. and associated rhizosphere bacterial communities. Environ. Sci. Pollut. Res. 24 (20), 16735–16750.
Qian, H., Hu, H., Mao, Y., Ma, J., Zhang, A., Liu, W., et al., 2009. Enantioselective phytotoxicity of the herbicide imazethapyr in rice. Chemosphere 76 (7), 885–892.
Qian, H., Wang, R., Hu, H., Lu, T., Chen, X., Ye, H., et al., 2011a. Enantioselective phytotoxicity of the herbicide imazethapyr and its effect on rice physiology and gene transcription. Environ. Sci. Technol. 45 (16), 7036–7043.
Qian, H., Lu, T., Peng, X., Han, X., Fu, Z., Liu, W., 2011b. Enantioselective phytotoxicity of the herbicide imazethapyr on the response of the antioxidant system and starch metabolism in *Arabidopsis thaliana*. PLoS ONE 6 (5), e19451.
Qian, H., Han, X., Zhang, Q., Sun, Z., Sun, L., Fu, Z., 2013. Imazethapyr enantioselectively affects chlorophyll synthesis and photosynthesis in *Arabidopsis thaliana*. J. Agric. Food Chem. 61 (6), 1172–1178.
Qian, H., Han, X., Peng, X., Lu, T., Liu, W., Fu, Z., 2014. The circadian clock gene regulatory module enantioselectively mediates imazethapyr-induced early flowering in *Arabidopsis thaliana*. J. Plant Physiol. 171 (5), 92–98.
Qian, H., Tsuji, T., Endo, T., Sato, F., 2014. PGR5 and NDH pathways in photosynthetic cyclic electron transfer respond differently to sublethal treatment with photosystem-interfering herbicides. J. Agric. Food Chem. 62 (18), 4083–4089.
Qian, H., Lu, H., Ding, H., Lavoie, M., Li, Y., Liu, W., et al., 2015a. Analyzing *Arabidopsis thaliana* root proteome provides insights into the molecular bases of enantioselective imazethapyr toxicity. Sci. Rep. 5, 11975.
Qian, H., Li, Y., Sun, C., Lavoie, M., Xie, J., Bai, X., et al., 2015b. Trace concentrations of imazethapyr (IM) affect floral organs development and reproduction in *Arabidopsis thaliana*: IM-induced inhibition of key genes regulating anther and pollen biosynthesis. Ecotoxicology 24 (1), 163–171.
Qu, Q., Zhang, Z., Li, Y., Zhou, Z., Ye, Y., Lu, T., et al., 2019. Comparative molecular and metabolic responses of wheat seedlings, (*Triticum aestivum* L.) to the imazethapyr enantiomers S-IM and R-IM. Sci. Total Environ. 692, 723–731.
Shi, Y., Zhang, J., Li, H., Li, M., 2018. Butanediol-enhanced heat tolerance in *Agrostis stolonifera* in association with alteration in stress-related gene expression and metabolic profiles. Environ. Exp. Bot. 153, 209–217.
Souza, R.D., Ambrosini, A., Passaglia, L.M., 2015. Plant growth-promoting bacteria as inoculants in agricultural soils. Genet. Mol. Biol. 38 (4), 401–419.
Sun, C., Chen, S., Jin, Y., Song, H., Ruan, S., Fu, Z., et al., 2016. Effects of the herbicide imazethapyr on photosynthesis in PGR5-and NDH-deficient *Arabidopsis thaliana* at the biochemical, transcriptomic, and proteomic levels. J. Agric. Food Chem. 64 (22), 4497–4504.
Tan, W., Liang, T., Li, Q., Du, Y., Zhai, H., 2014. The phenotype of grape leaves caused by acetochlor or fluoroglycofen, and effects of latter herbicide on grape leaves. Pest. Biochem. Physiol. 114, 102–107.
Thijs, S., Sillen, W., Rineau, F., Weyens, N., Vangronsveld, J., 2016. Towards an enhanced understanding of plant-microbiome interactions to improve phytoremediation: engineering the metaorganism. Front. Microbiol. 7, 341.
Vorholt, J.A., 2012. Microbial life in the phyllosphere. Nat. Rev. Microbiol. 10 (12), 828.
Xia, H., Li, S., Ma, L., Zhu, Q., 2014. Influence of Cu stress on chlorophyll fluorescence parameters of *Iris tectorum* maxim. J. HN. Agri. Sci. 43 (9), 79–82.
Zhang, M., Lu, T., Paerl, H.W., Chen, Y., Zhang, Z., Zhou, Z., et al., 2019. Feedback regulation between aquatic microorganisms and the bloom-forming cyanobacterium *Microcystis aeruginosa*. Appl. Environ. Microbiol. 85 (21) e01362–19.
Zhu, X., Lei, G., Wang, Z., Shi, Y., Braam, J., Li, G., Zheng, S., 2013. Coordination between apoplastic and symplastic detoxification confers plant aluminum resistance. Plant Physiol. 162 (4), 1947–1955.